EFFECTS OF COLD PLASMA TREATMENT ON INTERLAYER BONDING STRENGTH IN FUSED FILAMENT FABRICATION (FFF) PROCESS

A Thesis

by

CHIN-CHENG SHIH

Submitted to the Office of Graduate and Professional Studies of
Texas A&M University
in partial fulfillment of the requirements for the degree of

MASTER OF SCIENCE

Chair of Committee,	Li-Jung Tai
Committee Members,	Jyhwen Wang
	Jaime Grunlan
	David Staack
Head of Department,	Andreas Polycarpou

May 2019

Major Subject: Mechanical Engineering

ABSTRACT

Fused Filament Fabrication (FFF) is the most popular additive manufacturing method because of its numerous capabilities and relatively low cost. This comes with a trade off as FFF printed parts are typically weak in the layer deposition direction due to insufficient interlayer bonding. This research adopts the method of cold plasma treatment and investigates the potential enhancement of interlayer bonding by altering the printed surface prior to the deposition of the next layer. Polylactic acid (PLA) is used as the printing material, due to its ubiquity in industry. The bonding strength is measured by the shear bond strength test. The results show that bond strength improved over 100% with 30 s of treatment and over 50% with 300 s of treatment. A mechanically polished surface is also included in the comparison for the high surface wettability, but the result shows no improvement. This indicates that wettability may not be the dominant mechanism for enhanced bonding after treatment.

ACKNOWLEDGEMENTS

I would like to thank my committee chair, Dr. Bruce L. Tai, and my committee members, Dr. Jywen Wang, Dr. Jaime Grunlan, and Dr. Davide Staack for their guidance and support throughout the course of this research.

Thanks also go to my friends and colleagues and the department faculty and staff for making my time at Texas A&M University and in the United States a great and enjoyable experience.

Finally, thanks to my parents and sister for their support and encouragement.

CONTRIBUTORS AND FUNDING SOURCES

Contributors

This work was supervised by a thesis committee consisting of Dr. Bruce L. Tai [advisor] and Dr. Jaime Grunlan, and Dr. David Staack of the Department of Mechanical Engineering and Dr. Jyhwen Wang of the Department of Engineering Technology and Industrial Distribution.

The cold plasma system used in this research was provided by Dr. David Staack from Plasma Engineering and Non-equilibrium Processing Laboratory and assisted by his PhD students, Matthew Burnette and Christopher Campbell.

All other work conducted for the thesis was completed by the student independently.

Funding Sources

This research was not supported by any funding source.

NOMENCLATURE

3D	Three-dimensional
ABS	Acrylonitrile-butadiene-styrene
AM	Additive Manufacturing
ASTM	American Society for Testing and Materials
atm	Atmospheric pressure
CAD	Computer-Aided Design
CLIP	Continuous Liquid Interface Production
CNTs	Carbon Nanotubes
CPT	Cold Plasma Treatment
CPT30	Cold Plasma Treatment for 30 seconds
CPT300	Cold Plasma Treatment for 300 seconds
DAQ	Data Acquisition
DBD	Dielectric Barrier Discharge
DC	Direct Current
DLP	Digital Light Processing
DOD	Drop-On Demand
EBM	Electron Beam Melting
EDM	Electrical Discharge Machining
FFF	Fused Filament Fabrication
FDM	Fused Deposition Modeling

K	Kevin temperature
kHz	Kilo Herz
KMW	Low Molecular Weight
kV	Kilo Volt
LENS	Laser Engineered Net Shaping
LOM	Lamination Objective Manufacturing
s	Second
N	Newton
ns	Nanosecond
MJF	Material Jet Fusion
NPP	Nanosecond Pulsed Plasma
P	Polished
P+CPT	Polished and Cold Plasma Treatment
PLA	Polylactic acid
PTFE	Polytetrafluoroethylene
Ra	Average of the roughness
SDL	Selective Deposition Lamination
SLS	Selective Laser Sintering
SLM	Selective Laser Melting
UAM	Ultrasonic Additive Manufacturing
UTS	Ultimate Tensile Strength
uPP	Microsecond Pulsed Plasma

TABLE OF CONTENTS

Page

LIST OF FIGURES

Page

LIST OF TABLES

Page

CHAPTER I

INTRODUCTION*

1.1 Additive Manufacturing (AM)

Additive Manufacturing (AM), as known as 3D Printing, has gained huge popularity in recent years as it is able to directly and rapidly transform digital models into physical objects [1-4]. The fact that AM is able to build parts with complex geometries and has high production flexibility for customized designs has drawn attentions from many industries including aerospace, automobile, healthcare, and etc. In fact, AM is an umbrella term representing various type of technologies that build three-dimensional parts by adding material together typically layer by layer, as opposed to subtractive manufacturing that produces parts through material removal. Many AM technologies have been developed over the past few decades and they can be categorized into several types as shown in Table 1.

*Part of this chapter is reprinted from "Effects of cold plasma treatment on interlayer bonding strength in FFF process" by C.-C. Shih, M. Burnette, D. Staack, J. Wang, and B. L. Tai, 2019. *Additive Manufacturing* 25, 104-111, Copyright 2019 by Elsevier. No permission is required.

Table 1 AM Technologies

Material extrusion	Fused Filament Fabrication (FFF)
Vat photopolymerization	Stereolithography (SLA) Digital Light Processing (DLP) Continuous Liquid Interface Production (CLIP)
Powder bed fusion	Selective Laser Sintering (SLS) Selective Laser Melting (SLM) Electron Beam Melting (EBM) Multi Jet Fusion (MJF)
Binder jetting	Binder Jetting
Material jetting	Drop-On-Demand (DOD)
Direct energy deposition	Laser Engineered Net Shaping (LENS)
Sheet lamination	Lamination Object Manufacturing (LOM) Selective Deposition Lamination (SDL) Ultrasonic Additive Manufacturing (UAM)

1.2 Fused Filament Fabrication (FFF)

Fused Filament Fabrication (FFF), or called Fused Deposition Modeling (FDM), is an extrusion-based AM technology, invented in the 1990s [5]. In FFF, as shown in Figure 1, thermoplastic material in a form of filament is heated to a temperature above its melting point and then deposited by a motor-controlled extrusion head onto a platform (a.k.a. printing bed) to create a two-dimensional layer according to an input sliced digital model. After a layer is printed, the printing bed moves down (or extrusion head moves up depending on machine configurations) in z-direction for clearance and then the extruder prints a new layer on top of the deposited layer. Each printed layer fuses with its neighboring layers through thermal diffusion for permanent bonding. The printing process repeats until the entire model is built. Due to its convenience, various option of materials

and easy accessibility of machines, FFF has become the most used AM method in both academia and industry for rapid prototyping.

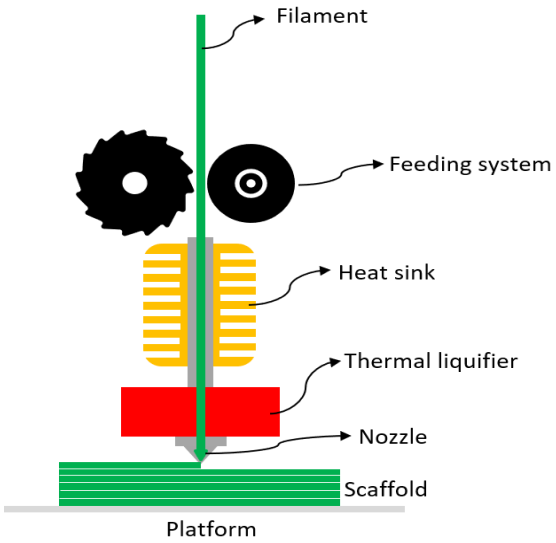

Figure 1 Scheme of FFF process

1.3 Anisotropy of FFF parts

To translate FFF technology to more applications, people have tried to utilize FFF for fabrication of functional and end-use parts, for example, in aerospace [6], automotive [7] and medical [8]; however, most of the work is still in the phase of research and development as the process has been hindered by a substantial issue for mechanical anisotropic properties exhibiting in FFF parts. A preliminary study on Ultimate Tensile Strength (UTS) of FFF parts printed in three different orientations, X,

Y, and Z directions (shown in Figure 2), has been conducted by following ASTM D638 standard [9] and compared with bulk properties of pure PLA. The results, as shown in Figure 3, reveal that the bulk PLA possesses strongest properties among all and the ultimate tensile load in z-direction (referred to z-strength) is significantly weaker than that of in x-direction and in y-direction (referred to x-strength and y-strength, respectively). Furthermore, results from several literature on mechanical properties of FFF parts, in which tensile strength, flexural strength, compressive strength, fracture strength, and etc. in different orientations are tested [10-21], also present the same trend where the mechanical performances in build direction (z-direction) are all worse than those in non-build direction (x- and y-direction). Such defective properties dramatically affect the integrity, durability and functionality of FFF parts, limiting the utilization of FFF.

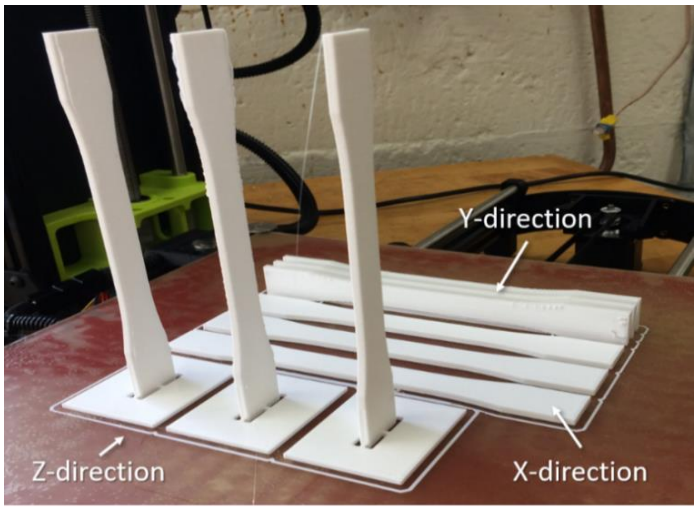

Figure 2 ASTM D638-14 specimens printed in three different orientations

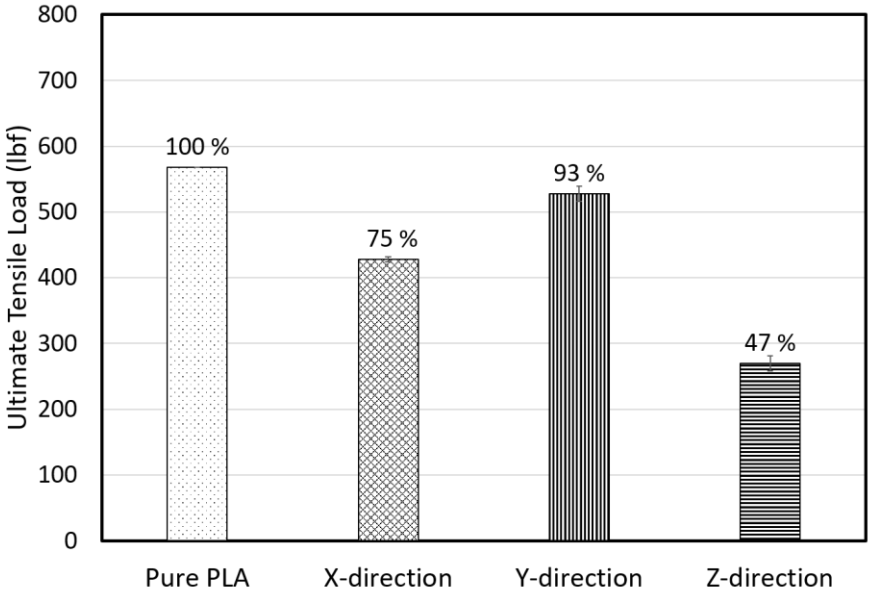

Figure 3 Ultimate Tensile Load of PLA specimens

Insufficient bonding between deposited layers has been considered the main cause for anisotropy of FFF parts. As printed layers solely rely on thermal diffusion for bonding, the bond quality is dominating the part strength in layer deposition direction. Several researchers investigate the mechanism of bond formation and mathematic models for strength prediction [22-26]. Ideally, thermal diffusion, under well-controlled conditions, can create strong bonds producing homogenous strength; however, it is difficult to be achieved in FFF process because of 1) insufficient thermal energy for diffusion due to rapid cooling of extruded material and the deposited layer [27], 2) limited contact area for bonding as vacancies between interlayers present [28, 29], and 3) inactive polymer surface for bonding [30].

1.4 Literature review

Many potential solutions have been proposed to improve interlayer bonding of FFF parts and they can be categorized into two types – internal and external methods. Internal methods focus on optimization of FFF process parameters such as raster orientation, layer thickness, air gap, etc. [27, 31-35]. Although tweaking printing parameters can potentially achieve maximum available strength of FFF parts, there is still a significant difference from injection molded parts as FFF-produced defects are not entirely eliminated. Some other researchers, therefore, are proposing external methods, which uses special materials, secondary processes, extra energy applications, or other aids as additional process to traditional FFF process, in order to improve interlayer bonding for enhanced part strength. They can be divided into two types: heating-based treatment and non-heating treatment.

1.4.1 Heating-based treatments

Heating-based methods, as its term implies, are to enhance bonding strength by applying external thermal energy in the process. Additional amount of heat induced into the process can promote thermal diffusion between printed layers, resulting in stronger bonds.

Shaffer et al. (2014) exposed 3D printed parts, printed with a special polylactic acid (PLA) blended with specific radiation sensitizers, to ionizing radiation. The results shows that the processed parts have better strength, thermo-mechanical properties, and solvent resistance due to crosslinking of the polymer [36].

Du et al. (2016) developed a laser-assisted FFF where two lasers were installed around the nozzle forming an elliptical focus area and heating up a printed layer before next deposition. The results showed an 195% increase in tensile strength due to extra thermal energy induced for material diffusion [37]. Not long later, *Ravi et al.* (2016) also used laser to locally heat up the region of a deposited layer (close to the nozzle) and then stronger bonding was also achieved [38], as illustrated in Figure 4 (a). Similar idea was applied again but, instead of using laser as a heat source, Kishore et al. (2017) preheated the printed layer before the next layer to a temperature close T_g using infrared lamps, resulting in better interlaminar strength and higher fracture energy [39], as illustrated in Figure 4 (b).

Wang et al. (2016) altered thermally expandable microspheres into FFF filaments for printing and performed heat treatment on the printed parts later. The part strength was improved, due to reduced voids in the part by the expanding of the microspheres as well as material sintering by heat treatment [40]. *Sweeney et al.* (2017) invented a special kind of FFF filaments coated with carbon nanotubes (CNTs), and applied microwaves provided from a dielectric barrier discharge (DBD) plasma to the printed material during printing. The weld fracture strength was improved by 275% due to strong localized heating of CNTs by microwaves [41], as illustrated in Figure 4 (c). *Jo et al.* (2018) heat treated FFF parts in a heated mold by forced convection heating with pressure applied, leading to better strength [42].

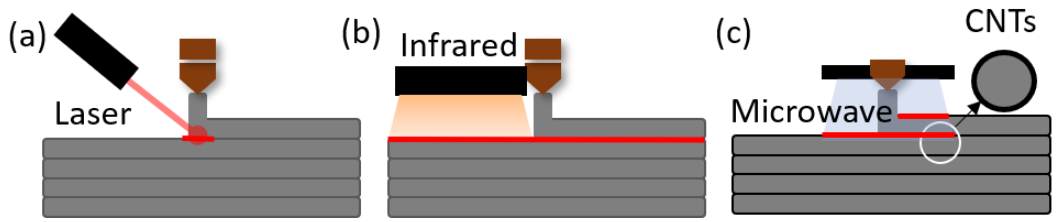

Figure 4 Thermal-induced FFF

1.4.2 Non-heating treatments

As opposed to heating-based treatments, non-heating treatments cover those methods using material blends, chemical reactions or mechanical fastening to achieve stronger interlayer bonding.

Lederle et al. (2016) processed FFF printing in a pure nitrogen chamber with no oxygen and the results show an improvement of 30% in tensile strength [43]. *Hiroyuki et al.* (2016) applied a plasma jet with helium gas to FFF printing for enhanced interlayer bonding [44], as illustrated in Figure 5 (a). *Abourayana et al.* (2017) used a barrel atmospheric plasma to treat polymer pellets before being made into filaments for FFF. The results show that the parts printed with the special filaments are stronger than those printed with regular filaments due to activation of bonding interfaces and removal of contaminations [45]. *Garg et al.* (2017) investigated the effects of chemical vapor treatment on FFF-printed parts. The acetone-vapor-treated parts showed a marginal reduction in strength while the surface finish was significantly improved [46]. *Nguyen et al.* (2018) integrated lignin, acrylonitrile-butadiene-styrene (ABS), acrylonitrile-butadiene rubber, and carbon fibers (CFs) to synthesize a new material with better

printability and bonding performance. 100% improvement on interlayer adhesion strength was achieved as the synthesized material prompted to have better interdiffusion [47]. *Li et al.* (2018) applied pressure and ultrasonic vibration on 3D-printed parts and found both tensile and bending strengths were increased after the process [48], as illustrated in Figure 5 (b). *Dudy et al.* (2018) used a mechanical method called z-pinning to improve part strength [49], as shown in Figure 5 (c). *Levenhagen et al.* (2018) induced additives with low molecular weight (LMW) onto FFF interfaces and results showed that stronger bonds were achieved as LMW additives required less thermal energy for diffusion [50, 51].

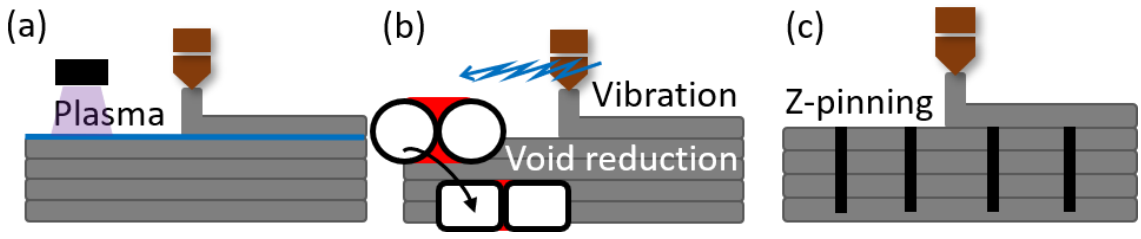

Figure 5 Non-heating methods

1.4 Proposed solution

Most of the aforementioned methods use heating to achieve better bonding strength. However, heating can inherently generate defects in printed parts. Localized or high-power heating, for example, can induce part distortion or warpage due to thermal stress, which is known to degrade part dimensional accuracy [52]. Furthermore, pre- and

post-processes require additional time and labor, which may reduce the simplicity and convenience of FFF 3D printing. For these reasons, this study presents an in-process and non-heating-based solution, named cold plasma treatment (CPT), to enhance the bonding strength while minimizing heat-induced distortion and defects. Schematic of CPT is illustrated in Figure 6. CPT is a surface modification technique that utilizes a high voltage and low current non-equilibrium plasma discharge to chemically and physically alter surface properties (to the depth of 50 – 500 Å) [53, 54]. CPT are operated at atmospheric pressure in a non-equilibrium fashion characterized by high temperature electrons (up to 10,000^{o}C) and room temperature gas (20^{o}C-40^{o}C) [44]. Cold plasma applicators have various geometries configured to provide high voltages and low average currents [55]. Examples include: 1) corona discharge geometries with sharp tips powered by a high voltage DC power, and with an incomplete breakdown of the discharge gap [56, 57]; 2) dielectric barrier discharges (DBD), in which one or both high voltage electrodes are covered by an electrically insulating barrier to limit currents [58-60], 3) nanosecond pulsed plasma (NPP) and microsecond pulsed plasma (μPP) discharges where the external circuit is used to limit discharge power; and 4) plasma jets, in which convection of a gas (typically a noble gas) along with its electrical and transport properties help maintain the non-equilibrium [61]. These various sources have similar global plasma properties, although they vary significantly in their cost, efficiency and ability to maintain non-equilibrium over a wide variety of operating conditions. Aspects of these configurations can also be combined for greater efficacy. Historically DBDs and coronas have been used since the early 1900's in industrial applications for surface

modifications. Jets and NPP have gain popularity in research in the last 20 years. This research adopts a different plasma source which combines aspects of a NPP, a jet, a corona geometry, and a DBD to create a highly non-equilibrium glow discharge, as shown in Figure 7.

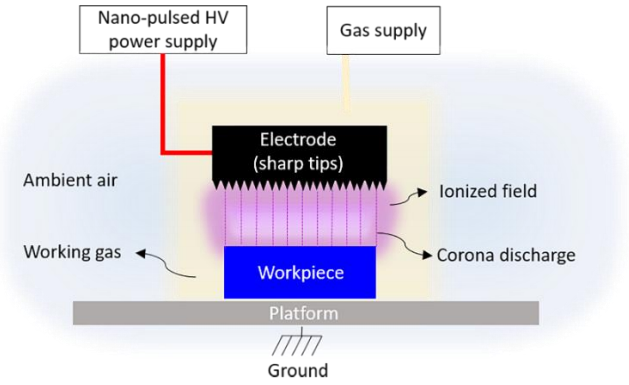

Figure 6 Schematic of CPT process
Reprinted from "Effects of cold plasma treatment on interlayer bonding strength in FFF process" by C.-C. Shih, M. Burnette, D. Staack, J. Wang, and B. L. Tai, 2019. Additive Manufacturing 25, 104-111, Copyright 2019 by Elsevier. No permission is required.

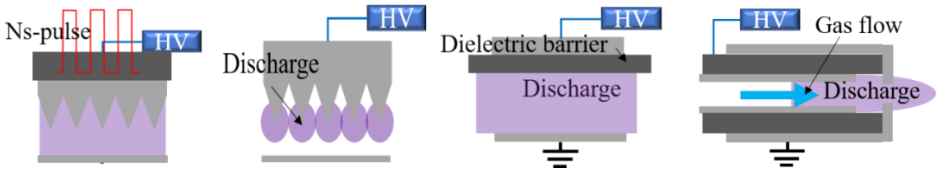

Figure 7 Plasmas in CPT: NPP, Corona, DBD, and Plasma Jet (left to right)

CPT has been widely used in industry to increase the surface energy of various polymers for enhanced adhesion or bonding [62]. The two major mechanisms of CPT

that enhance surface adhesion involve polar group introduction and polymer chain scission. As CPT triggers oxidation on the polymer surfaces, polar groups with high surface energy such as carbonyl groups will form on surfaces, resulting in a better wettability. This improved wettability prompts liquid to spread along the surface, providing a larger contact area for diffusion bonding. Since polymers are synthesized from numerous long molecular chains joining end to end with only a few dangling ends at the surfaces for further bonding, their adhesion and wettability are poor. CPT can relieve this issue by breaking the polymer chains producing loose ends for bonding by bombarding the polymer surfaces with electrons during the plasma discharge and other radicals. Furthermore, polymetric scission products prompt better interfacial flow and inter-diffusion due to their lower molecular weight, lower glass transition temperature, and lower viscosity, so treated surfaces require less thermal energy (lower temperature) for bonding [30, 63, 64].

The objective of this research is to determine the improvement of interlayer bonding of FFF via CPT and to investigate the dominant mechanism of enhanced bonding. To achieve this, different treatment times along with mechanically polished and unpolished samples are compared in this work. Mechanical polishing is included as it also changes the surface wettability due to the interactions between liquid surface tension and surface texture. This is, therefore, used to study the significance of wettability in interlayer bonding strength alone as well as to analyze the combined effect with CPT.

CHAPTER II

INTERLAYER BONDING AND PLASMA TREATMENT[*]

2.1 Measurements of interlayer bonding strength

Polymer adhesion has been fundamentally and practically studied in both academia and industries as adhesion is commonly used everywhere nowadays. To evaluate the performance of adhesion, many direct techniques for bonding test have been developed and standardized. Three common standards for plenary polymer adhesion system are found, including lap-shear test, T-peel test, and pull-off test, as shown in Table 2.

However, although those listed bonding test standards are maturely practiced in industries, they are found to be difficult to evaluate interlayer bonding strength of FFF-printed layers for two reasons. Firstly, it is challenging to break through the targeted bonding interface accurately without damaging the main structure of specimens. FFF-produced diffusion bonding (as known as "autohesion" or "thermal healing") is relatively strong compared to normal adhesive bonding ("gluing"), so the separation force of the interface could be very high, leading to deformation, distortion, or breakage of testing specimens during the test. This situation may result in incorrect data. An

[*]Part of this chapter is reprinted from "Effects of cold plasma treatment on interlayer bonding strength in FFF process" by C.-C. Shih, M. Burnette, D. Staack, J. Wang, and B. L. Tai, 2019. *Additive Manufacturing* 25, 104-111, Copyright 2019 by Elsevier. No permission is required.

example can be seen in Figure 8 where the FFF-printed specimens were distorted and randomly damaged when tested under ASTM D3163 standard using a tensile tester. ASTM D1876 is also considered inapplicable for the same reason as the thin flanges in its specimen design can suffer from such failures due to strong separation force. Secondly, facture may not happen along the targeted interface but its neighboring layers if those layers are weaker. This scenario can be observed in Figure 9 where the FFF specimens were tested by following ASTM D4541 and none of them broke at the targeted interfaces.

Table 2 Common methods for adhesion test

Standard	Type	Schematic
ASTM D3163 [65]	Lap shear joint test	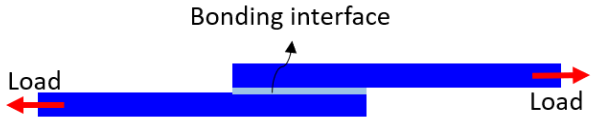
ASTM D1876 [66]	T-peel test	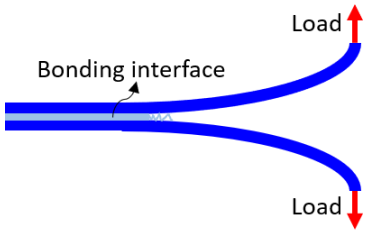
ASTM D4541 [67]	Pull-off test	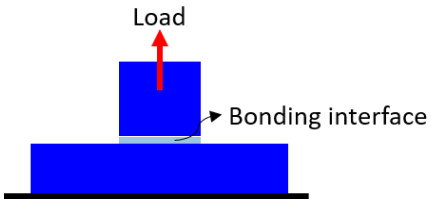

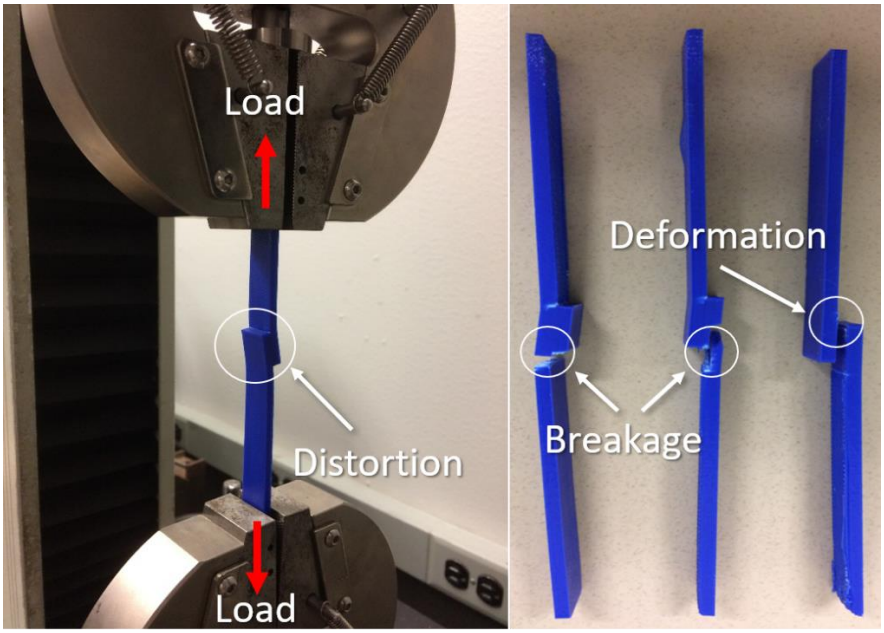

Figure 8 ASTM D3163 bonding test on FFF-printed specimens

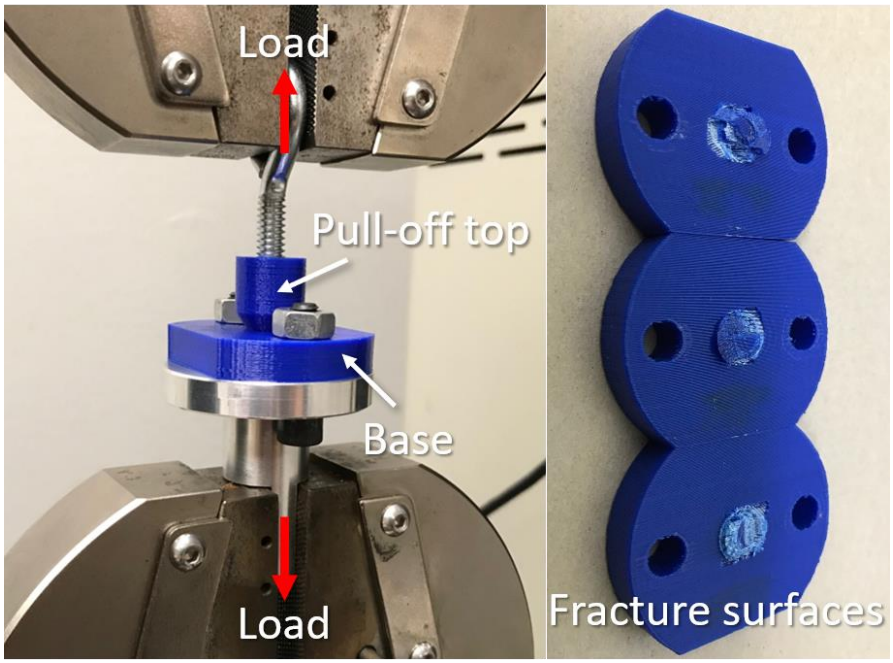

Figure 9 ASTM D4541 bonding test on FFF-printed specimens

As a result, in this study, a non-standard method was adopted from a shear bond strength test of dental composites [68], namely shear bond test, as shown in Figure 10. Instead of using tension force, the shear bond method uses an insert to cut through a targeted bonding interface and shear off the top layer. The fracture is more predictable with this method as its path and propagation can be controlled by the insert motion. Also, the geometry of its specimen is relatively small and easier to be made as compared to those aforementioned standard tests.

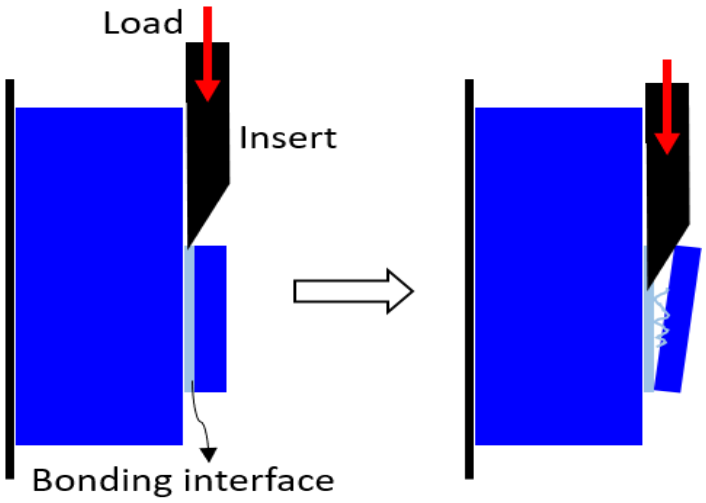

Figure 10 Schematic of shear bond test method

2.2 Specimen preparation and shear bond test setup

Polylactic acid (PLA) was selected as the testing material as it is a common thermoplastic in FFF with widespread accessibility and less dimensional distortion after

printing. FFF 3D printer, Dreamer (Flashforge, Zhejiang, China) and standard 1.75 mm PLA filaments in blue were used to fabricate specimens. Slicing software, Simplify3D (Simplify3D, Cincinnati, OH), was used to arrange the printing parameters and tool paths. The design of specimen geometry included two sections, substrate, and top layer, as shown in Figure 11. The substrate was 20 mm by 12.5 mm by 12.5 mm, and the top layer was a thin layer meant to be sheared off to determine the bonding strength. The specimens were made following three-step procedures. Once the substrate was printed, the printing process was paused, and the entire printing platform was removed to conduct surface treatment away from the machine in order to avoid contamination and electromagnetic interference from the CPT. After the treatment, the platform was installed back in the 3D printer to continue the printing of the top layer. This way ensured a consistent layer thickness across the treated interfacial layer. If the substrate and top layer were printed separately, inconsistent layer thickness could be created due to machine zeroing error. In addition, the re-installed platform must stay in the machine for at least 30 mins to allow the printed part to reach a steady-state temperature around 38.3 °C in order to avoid temperature discrepancy with the baseline printing. Note the temperature-induced dimensional error is negligible given a small thermal expansion coefficient (4.1×10^{-7} m/m) of PLA and little shrinkage. Finally, the complete specimen was sent to the testing apparatus.

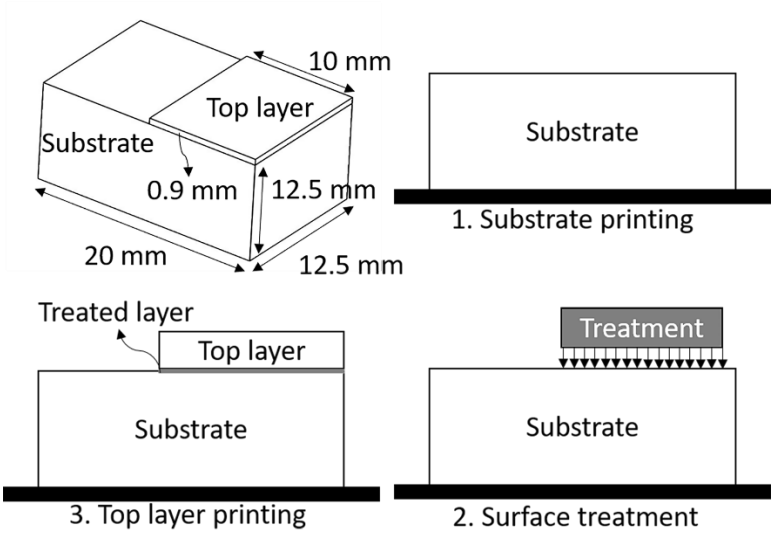

Figure 11 Specimen dimension and preparation for the shear bond test
Reprinted from "Effects of cold plasma treatment on interlayer bonding strength in FFF process" by C.-C. Shih, M. Burnette, D. Staack, J. Wang, and B. L. Tai, 2019. Additive Manufacturing 25, 104-111, Copyright 2019 by Elsevier. No permission is required.

A self-developed apparatus, shown in Figure 12, used a sharp tip to shear and peel the top layer off from the substrate. A close-up observation on the contact of the peeling tip and specimen layers was also performed to ensure the nose of the tip is small enough and able to stick in between the layers, as shown in Figure 13. The shearing force was measured using a dynamometer that could capture a rapid force response. The measured force was used to represent the interlayer bonding strength. Other components in the apparatus included a fixture on the dynamometer to secure the specimen and a numerically controlled linear slider for a quasi-static peeling rate at 12.5 mm/min. The data acquisition (DAQ) system was used to transfer high-frequency data at a sample rate of 10 Hz from the dynamometer to the computer in real time.

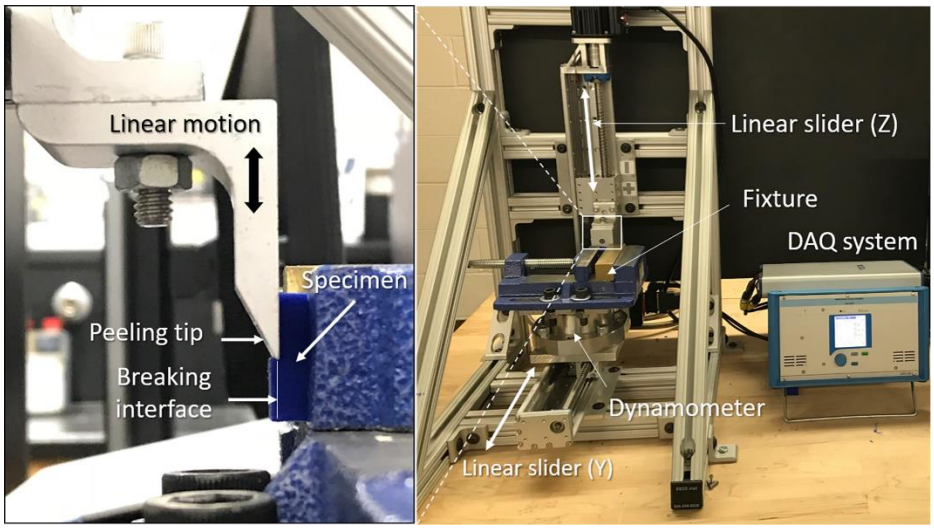

Figure 12 The setup for shear bond test to measure the interlayer bonding strength Reprinted from "Effects of cold plasma treatment on interlayer bonding strength in FFF process" by C.-C. Shih, M. Burnette, D. Staack, J. Wang, and B. L. Tai, 2019. Additive Manufacturing 25, 104-111, Copyright 2019 by Elsevier. No permission is required.

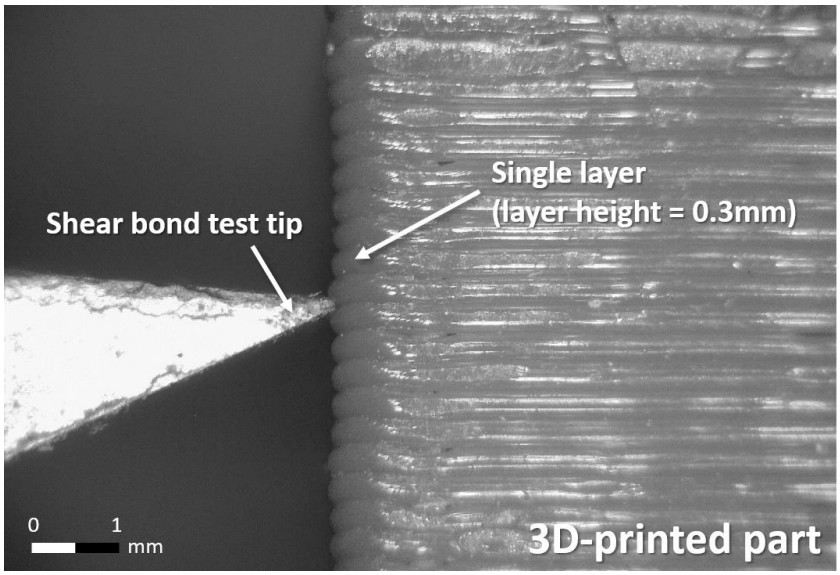

Figure 13 Microscopic observation on the peeling tip and layers

Using an untreated sample as the baseline, the four surface conditions are listed in Table 3. The results were expected to unveil the effects of CPT on interlayer bonding and the dominant bonding mechanism being wettability or the continuous cross-linking via polymer chain scission. The only variable in CPT was the treatment time. It was hypothesized that a longer treatment resulted in a stronger bonding; thus, two substantially different time durations, 30 s and 300 s, were selected. For mechanical polishing, only one grit size was selected since the main purpose was to test the effect of wettability (i.e. high vs. low) by altering the surface profile. Further, Test #4 was to check if combining polishing and CPT can result in a better performance than CPT alone. Each condition contained five specimens to ensure adequate statistical power for comparison. The details of the surface treatment procedures are presented in the next section.

Table 3 Four treatment conditions of specimens

Tests	Conditions	Notations
Short CPT	30 s plasma treatment	CPT30
Long CPT	300 s plasma treatment	CPT300
Polishing	#180 grits	Polished
Polishing+CPT	#180 grits and then 300 s treatment	P+CPT

2.2 Surface treatments and conditions

The configuration of the CPT is shown schematically in Figure 6. The CPT system is composed of a power supply, electrode, electrode holder, adjustable platform,

and gas supply. A high voltage nanosecond pulser, FPG 30-N (FID GmbH, Burbach, Germany), was used as the power supply with capabilities of outputting a maximum voltage of 30 kV, pulse width of 3 ns, and a maximum pulse frequency of 10 kHz. A stainless-steel electrode composed of sharp tips and gas spacers was connected to the power supply to produce a dielectric barrier discharge. The sharp tips were made of multiple 0.6 mm thin sheets with a serrated profile machined by electrical discharge machining (EDM), as shown in the close-up view in Figure 14. The tips are spaced every 0.5 mm across a sheet with 0.4 mm inter-sheet spacing. The spacers were machined by EDM with a special configuration and inserted between the serrated sheets to allow gas flow. The PTFE (Teflon) block provided housing for the electrode and for transporting the working gas to the electrode. The array of sharp tips is essential to producing large and uniform plasma discharge, and the gas flow kept the temperature low due to the electrical and thermal properties of helium and forced convection.

The following working parameters, shown in Table 4, were set to be fixed across all samples in this study. The CPT was working under ambient pressure and at room temperature and humidity (around 22 °C and 60% humidity). The voltage was set at 20 kV, and the frequency was set at 2 kHz. Helium gas was used as the working gas. The measured vibrational temperature was found to be around 3100 K and the rotational temperature was approximately 460 K in this plasma using the 2^{nd} positive system of nitrogen and SpecAir for modeling [69, 70]. The discharge distance, the gap between the electrode and the working part, was approximately 1 mm from the tips for the best performance, beyond or below which the plasma did not initiate or became too intense

on the surface. In this study, the only independent variable is the discharge time (0, 30 s, and 300 s) to observe the effect on bonding performance.

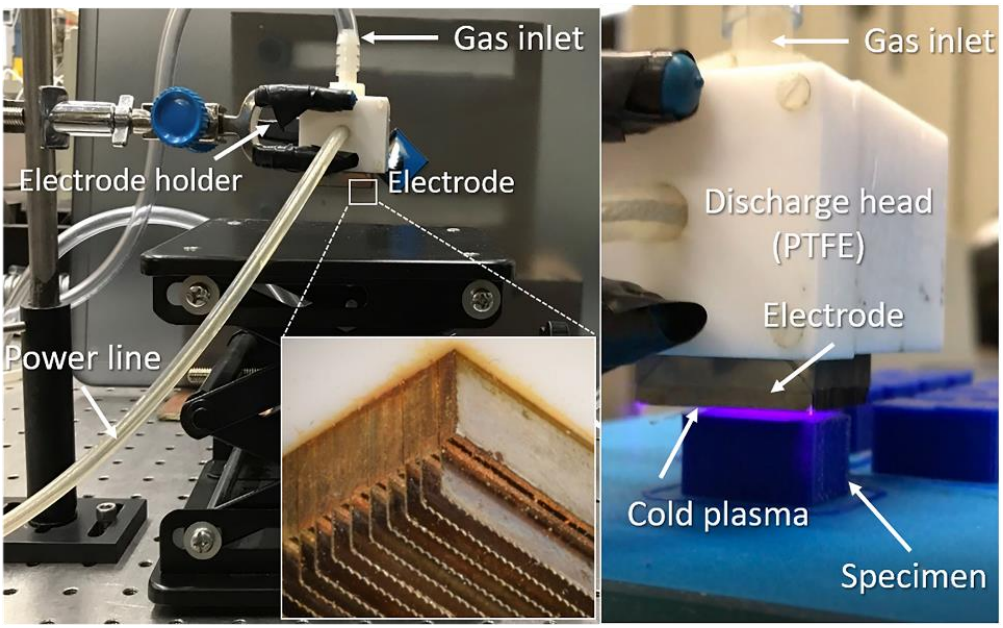

Figure 14 The CPT system configuration
Reprinted from "Effects of cold plasma treatment on interlayer bonding strength in FFF process" by C.-C. Shih, M. Burnette, D. Staack, J. Wang, and B. L. Tai, 2019. Additive Manufacturing 25, 104-111, Copyright 2019 by Elsevier. No permission is required.

Table 4 The working parameters of CPT

Plasma Working Parameters	
Voltage (kV)	20
Frequency (kHz)	2
Gas (L/min)	2.5 (Helium)
Discharge distance (mm)	~1
Pressure	Ambient (1 atm)
Temperature	Room (22 ˚C)

The mechanical polishing was conducted with sandpaper manually without directionality. Sandpaper with a grit size of 180 was attached on a flat guide plate to grind the target surface gently to ensure an even and uniform surface. The polished surface and residue were cleaned with high-pressure compressive air. The surface roughness was checked using an optical 3D profilometer, InfiniteFocus (Alicona, Graz, Austria), and the default cutoff length of 0.212 mm at multiple spots until consistent roughness value (Ra) was reached and no extrusion marks were observed, as shown in Figure 15. Additionally, the removed surface layer was controlled at 0.1 mm and this height difference was programmed into the 3D printer to compensate for the following layer. Note that the polished surface, in fact, became rougher in terms of Ra (4.98 vs. 1.89 μm) because the surface profile transformed from waviness to the roughness scale.

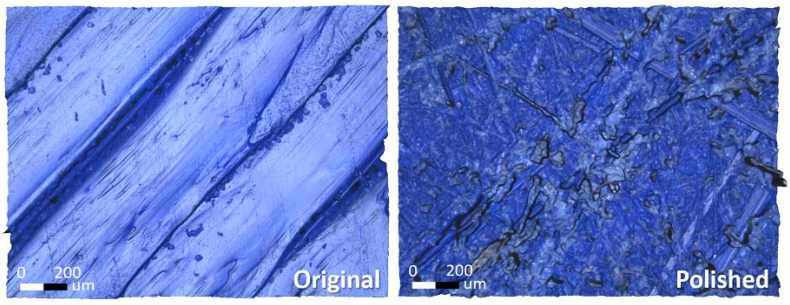

Figure 15 Surface geometries of (left) as-printed and (right) polished PLA
Reprinted from "Effects of cold plasma treatment on interlayer bonding strength in FFF process" by C.-C. Shih, M. Burnette, D. Staack, J. Wang, and B. L. Tai, 2019. Additive Manufacturing 25, 104-111, Copyright 2019 by Elsevier. No permission is required.

Before conducting the shear bond test, the specimens were tested for their wettability by the contact angle of water droplet based on ASTM standard (D7334-08) [71]. Figure 16 shows the results of the contact angle. The purpose was to ensure that both CPT and mechanical polishing produced high surface wettability. As seen, the untreated baseline surface had a contact angle higher than 75°, that of CPT is around 40-45°, and that of the mechanically polished surface is less than 10°. It is important to note that the wetting effect appears very quickly after CPT and remains nearly constant with respect to treatment time. Both the 30 s and 300 s treatments have a similar contact angle. The mechanically polished surface had the best wetting condition among all, and thus was ideal to be used for comparing the wettability effect in bonding strength.

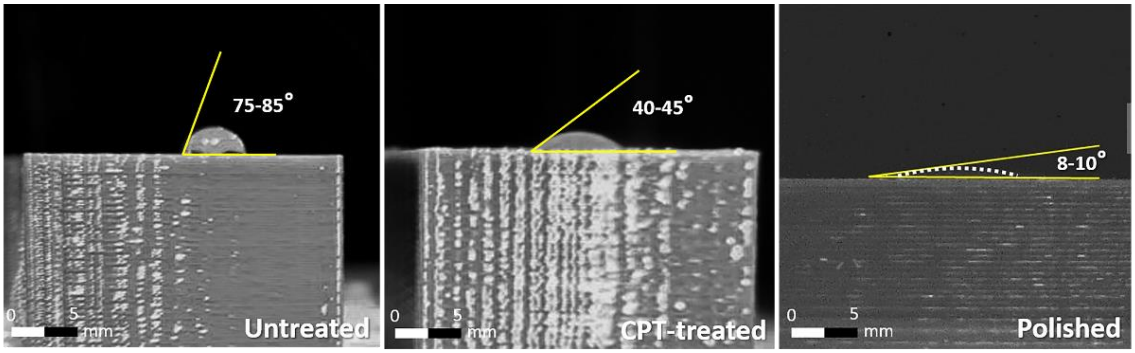

Figure 16 Contact angles of untreated, CPT, and polished surfaces
Reprinted from "Effects of cold plasma treatment on interlayer bonding strength in FFF process" by C.-C. Shih, M. Burnette, D. Staack, J. Wang, and B. L. Tai, 2019. Additive Manufacturing 25, 104-111, Copyright 2019 by Elsevier. No permission is required.

CHAPTER III

EXPERIMENTAL RESULTS AND DISCUSSION*

3.1 Untreated vs. CPT30 vs. CPT300

The force data for the CPT30 and CPT300 samples from the shear bond tests are shown in Figure 17, where the peak force of each data represents the bonding strength. For comparison purposes, the untreated specimens are also plotted. As shown, the bonding strengths are significantly improved with CPT. The peak forces of both CPT30 (from 447 to 506 N) and CPT300 (from 272 to 380 N) are repeatedly greater than that of the baseline (from 113 to 237 N). In addition, the baseline specimens experience rapid force drop after the peak force, which indicates a fast crack propagation in brittle materials. In contrast, the force drops for the CPT specimens are progressive, indicating a higher toughness of the interface. Since the shearing rate is constant, the area below each curve represents the energy required to remove the entire top layer. Another interesting finding is that, in the comparison between CPT30 and CPT300 samples, the force values of CPT30 are greater than those of CPT300. This result shows that the bonding strength is not positively proportional to the treating time.

*Part of this chapter is reprinted from "Effects of cold plasma treatment on interlayer bonding strength in FFF process" by C.-C. Shih, M. Burnette, D. Staack, J. Wang, and B. L. Tai, 2019. *Additive Manufacturing* 25, 104-111, Copyright 2019 by Elsevier. No permission is required.

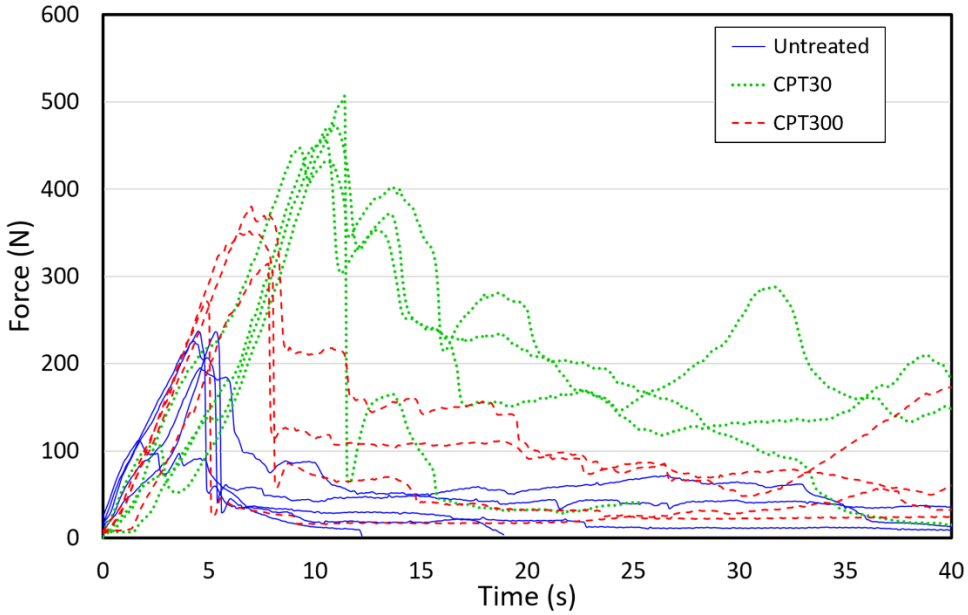

Figure 17 Force responses with respect to time - Untreated, CPT30, and CPT300 Reprinted from "Effects of cold plasma treatment on interlayer bonding strength in FFF process" by C.-C. Shih, M. Burnette, D. Staack, J. Wang, and B. L. Tai, 2019. Additive Manufacturing 25, 104-111, Copyright 2019 by Elsevier. No permission is required.

3.2 Untreated vs. CPT300 vs. Polished

To understand the role of wettability in bonding strength, three test results are studied and compared in Figure 18, including the baseline, CPT300, and the polished case. For clarification, the results of baseline and CPT specimens are retrieved from the same data set in the previous figure. As can be seen, the CPT300 specimens are the strongest among all. The polished ones, with forces ranging from 188 to 232 N, appear to be similar to the baseline in terms of the peak force and are overall weaker than CPT300. Also, the polished ones have a faster force reduction (after the peak) than those

of the baseline despite similar peak forces. This result indicates that mechanical polishing may reduce the bonding toughness.

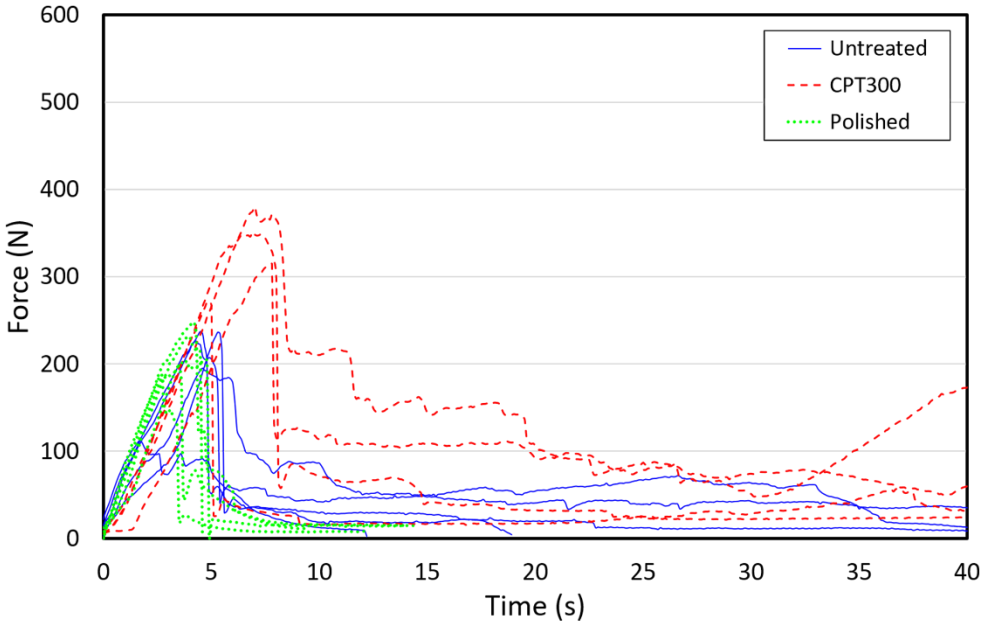

Figure 18 Force responses with respect to time - Untreated, CPT300, and Polished
Reprinted from "Effects of cold plasma treatment on interlayer bonding strength in FFF process" by C.-C. Shih, M. Burnette, D. Staack, J. Wang, and B. L. Tai, 2019. Additive Manufacturing 25, 104-111, Copyright 2019 by Elsevier. No permission is required.

3.3 Untreated vs. Polished vs. P+CPT

The third set of results, including baseline, polished, and P+CPT, are compared to investigate the combined effects of two treatments in this study, as shown in Figure 19. The results show no significant difference among all three tests in terms of peak forces. However, the continuous shearing forces of P+CPT indicate a slightly higher toughness than polished ones, while the baseline remains the toughest. These results

show that the negative effect of polishing can overwrite the enhanced adhesion from CPT. CPT cannot further improve the bonding strength after the surface is polished.

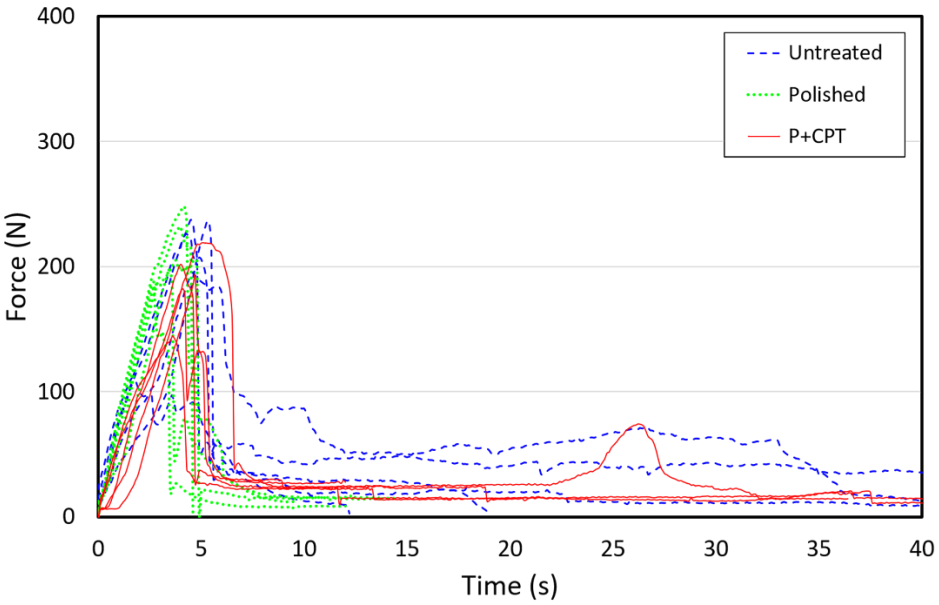

Figure 19 Force responses with respect to time - Untreated, Polished, and P + CPT
Reprinted from "Effects of cold plasma treatment on interlayer bonding strength in FFF process" by C.-C. Shih, M. Burnette, D. Staack, J. Wang, and B. L. Tai, 2019. Additive Manufacturing 25, 104-111, Copyright 2019 by Elsevier. No permission is required.

3.4 Overall comparison

The averages of the peak shear-bond forces of all tests are calculated and presented in Figure 20. The error bars represent the standard error. Based on statistical analysis, CPT300, CPT30, and the baseline are statistically different among each other (p-value < 0.05), whereas polished, P+CPT, and the baseline are considered not statistically different (p-value > 0.05). Considering the baseline bonding strength, CPT30 improves the bonding strength by 134% on average, followed by CPT300 at 63%.

In addition to the peak forces, total work done to fracture of each specimen across all conditions is also calculated based on the area under each force data curve, as shown in Figure 21.

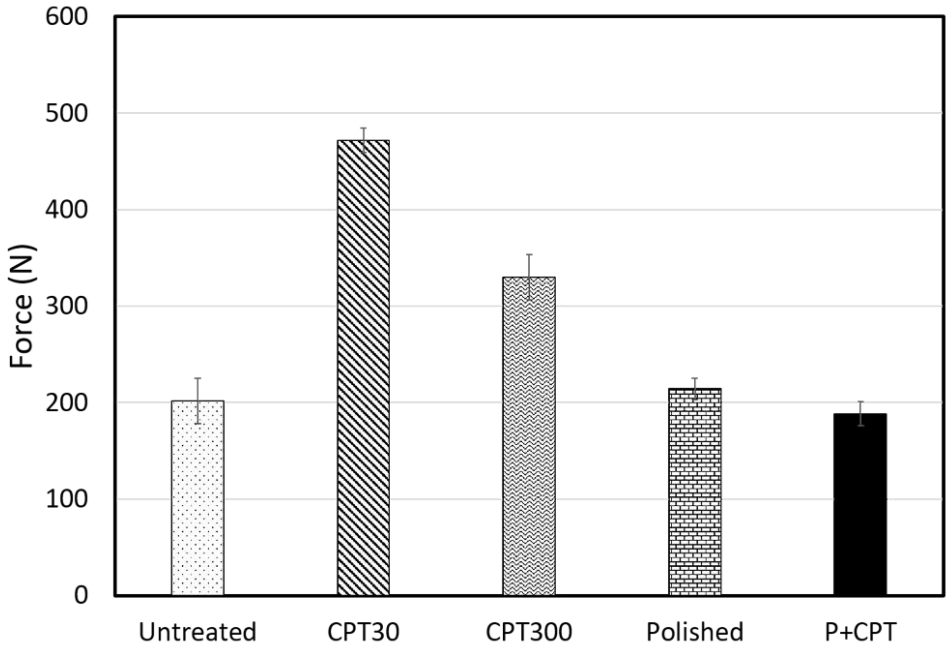

Figure 20 Comparison of the peak forces of all conditions
Reprinted from "Effects of cold plasma treatment on interlayer bonding strength in FFF process" by C.-C. Shih, M. Burnette, D. Staack, J. Wang, and B. L. Tai, 2019. Additive Manufacturing 25, 104-111, Copyright 2019 by Elsevier. No permission is required.

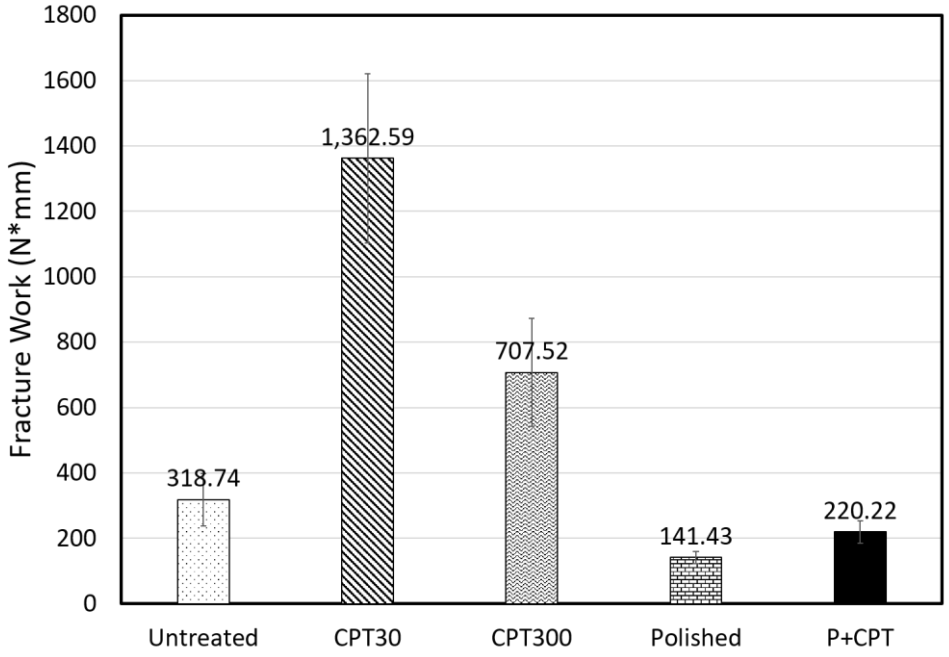

Figure 21 Comparison of total work done to fracture
Reprinted from "Effects of cold plasma treatment on interlayer bonding strength in FFF process" by C.-C. Shih, M. Burnette, D. Staack, J. Wang, and B. L. Tai, 2019. Additive Manufacturing 25, 104-111, Copyright 2019 by Elsevier. No permission is required.

3.5 Fracture surface microscopy

Lastly, the fracture surfaces were observed under an optical microscope to compare the treated effects on the interfaces, as shown in Figure 22. Stress whitening, also known as crazing, can be seen on both CPT specimens. Stress whitening occurs when thermoplastic polymers are under an excessive tensile load, which causes the formation of micro-voids due to the movement of molecular chains, thus changing the material refractive index [72]. Therefore, the degree of stress whitening can reflect the level of bonding force between layers after delamination. CPT 30 shows clear white striations that align with the deposited filament extrusions, indicating a strong bonding

between the deposited material and base layer. CPT 300 shows some stress whitening regions, but they are not as many and as well-distributed as those in CPT 30. Such a difference is the evidence of the lower bonding force of CPT 300. The untreated, polished, and P+CPT specimens show no stress whitening effect, indicating an easy separation of the top layer. The optical images agree with the force results obtained from the shear bond test in Figure 20. Note the small and scattered whitening spots in the polished and P+CPT samples were created by abrasives during the polishing process instead of layer separation during the shear bond test.

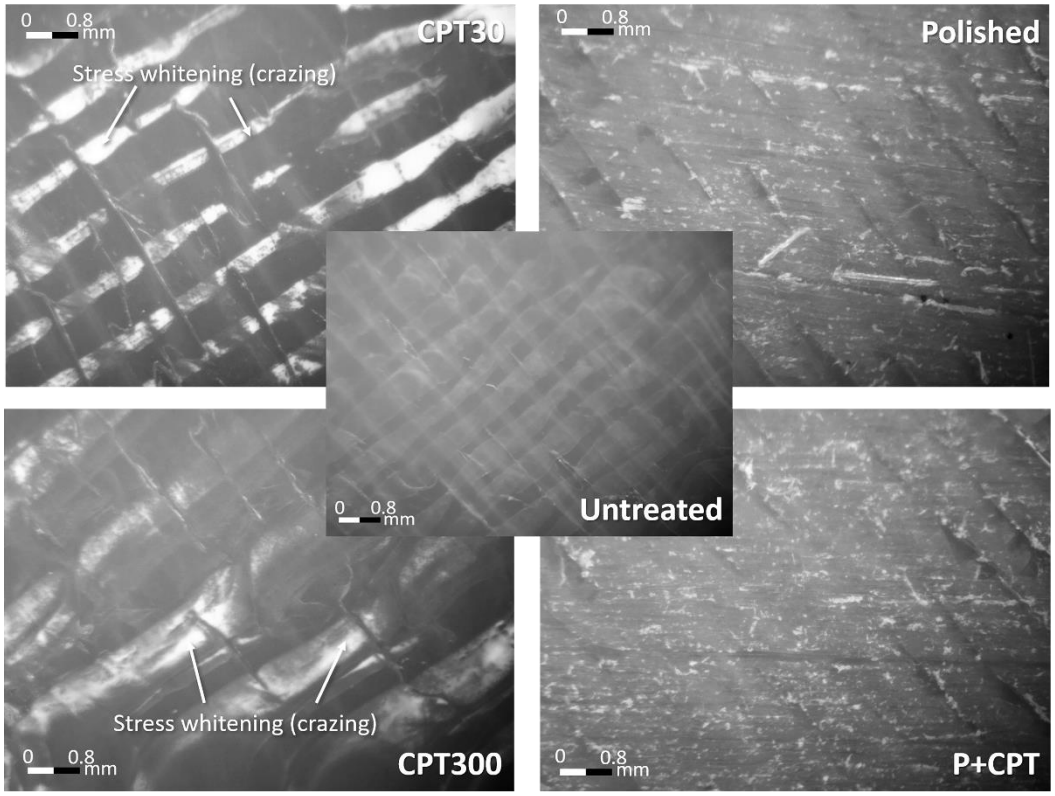

Figure 22 Fractured surfaces of untreated, CPT30, CPT300, Polished, and P + CPT
Reprinted from "Effects of cold plasma treatment on interlayer bonding strength in FFF process" by C.-C. Shih, M. Burnette, D. Staack, J. Wang, and B. L. Tai, 2019. Additive Manufacturing 25, 104-111, Copyright 2019 by Elsevier. No permission is required.

3.6 Discussion

As CPT can enhance interlayer bonding in FFF parts, determining an optimized treatment time is desired in order to achieve the best possible performance. According to the results, the specimens treated with shorter CPT are shown to have stronger bonding than the ones which underwent longer treatment. This may be due to polymer degradation caused by overtreatment. When a polymer surface is exposed to plasma, an oxidation layer can grow into the surface at a certain rate over time. As mentioned in Section 1, the oxidized surface is one of the key elements for enhanced surface energy; however, overgrowing the oxidized layer with an excessive thickness (up to 6 μm depending on the treatment time and parameters [30]) may negatively affect the treatment performance. The oxidization layer has a relatively low strength (due to lower molecular weight); thus, a thicker oxidation layer may become a weak intermediate layer that triggers fractures. Therefore, tuning the treatment time duration to reach a certain level of oxidation on target surfaces is an essential task for optimizing bonding strength based on the work-material and plasma parameters.

Another counterintuitive observation is that the wettability was not shown to dominate the bonding strength based on the results of the polished specimens. Unlike common adhesion cases such as paint coating and adhesive bonding that solely rely on chemical bonds, where the wettability (a spontaneous spread-out motion) plays a key role, the viscous or semi-solid polymer used in FFF can hardly deform without external forces. On the other hand, these external forces can overwrite the wettability effects.

When the melt is being laid down onto a surface, the surface is melted due to heat transfer and the surface geometry is "mowed." All while, the printing nozzle squeezes and compresses the melt while printing. These can all change the interfacial contact area significantly more than the wettability can alone.

To further look into the wettability effects, the structures of untreated and CPT300 specimens were observed under a microscope. As shown in Figure 23, the results show no or little to no difference between the untreated and treated specimens. In other words, the different initial wetting conditions do not change how the melt spreads on a surface in FFF. Therefore, the wettability may not be a major factor in CPT to enhance the bonding strength of FFF. This observation also explains why the polished surface does not exhibit any improvement despite having a high wettability.
Instead, mechanical polishing seems to worsen the bonding strength. This result may be explained by the removal of printing patterns (Figure 15) which are made of multiple single extrusion arrays. Such a pattern can potentially provide interlocking between layers through a 45˚/-45˚printing orientation and produce a larger contact area than a smooth surface. This hypothesis can be indirectly verified by the comparison between the polished and P+CPT cases. Although CPT can enhance polymer diffusion, the polishing process that removes the patterns may even out the effect of CPT, thus the overall bonding shows no increase.

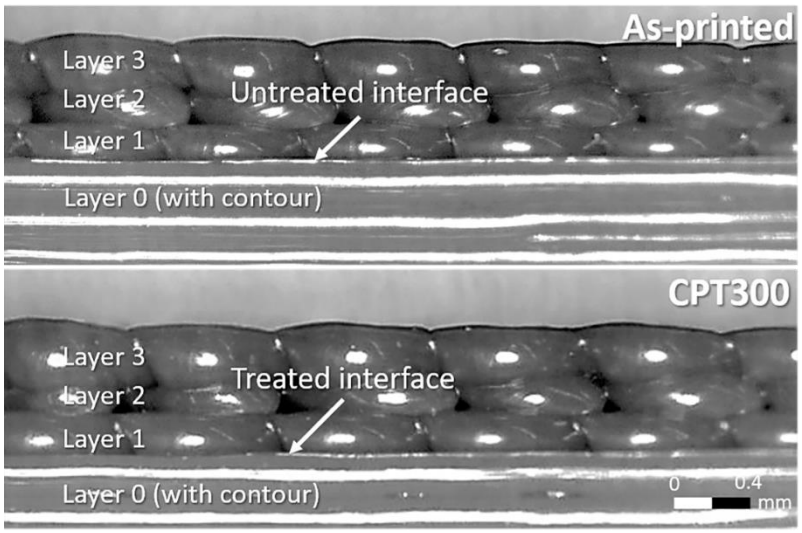

Figure 23 Mesostructures of the untreated and CPT300 specimens
Reprinted from "Effects of cold plasma treatment on interlayer bonding strength in FFF process" by C.-C. Shih, M. Burnette, D. Staack, J. Wang, and B. L. Tai, 2019. Additive Manufacturing 25, 104-111, Copyright 2019 by Elsevier. No permission is required.

Before concluding, there are several limitations applied to this work that should be mentioned. Firstly, the CPT effect is time sensitive and can degrade over time. Although the time between treatment and test was kept short, within 30 mins, the actual degradation of treated surfaces was not quantitatively measured. Generally, the plasma effect can last around 24 hours or longer [30], so the time interval is considered insignificant. Secondly, only one material was tested with a fixed plasma condition; thus, the quantitative effects of plasma on the bonding strength, such as treatment time, cannot be generalized. Finally, the comparison between the CPT and polished cases also involve the difference in surface roughness in addition to wettability (which are coupled together). The discussion on wettability effect is based on the assumption that surface interlocking is not dominant.

CHAPTER IV

SUMMARY*

5.1 Conclusions

This study determined the improvement of interlayer bonding strength of 3D printed PLA parts treated by cold plasma. A low-energy plasma system and shear bonding apparatus were specifically built to meet the needs of the experimental design. Based on the results, it was found that CPT can significantly increase the bonding strength by over 100%, which is likely to bring the z-direction strength closer to that of the x- and y-directions of the printed part. Longer treatment is not necessarily better, however, and there should exist an optimal treatment setting for different thermoplastics used. Another important finding is that the dominant mechanism for CPT to enhance the interlayer bonding is polymer scission instead of wettability. A counterpart specimen with a better wettability caused by mechanical polishing resulted in no improvement to weaker bonding.

This study has successfully demonstrated the positive effect of CPT in FFF while also unveiling possibly sophisticated mechanisms behind the CPT based 3D printing process. Before the optimization of CPT is possible, fundamental studies on both chemical, mechanical, and combined mechanisms are necessary.

---

*Part of this chapter is reprinted from "Effects of cold plasma treatment on interlayer bonding strength in FFF process" by C.-C. Shih, M. Burnette, D. Staack, J. Wang, and B. L. Tai, 2019. *Additive Manufacturing* 25, 104-111, Copyright 2019 by Elsevier. No permission is required.

5.2 Future work

5.2.1 Fundamental studies

Although the research reveals that the interlayer bonding of FFF printed layers can be significantly improved by the cold plasma treatment, the domaining mechanisms leading to the improvement remains unknown. As mentioned in Chapter I, there are four types of potential mechanisms that play roles in the cold plasma process contributing to bonding strength increase: 1) polymetric scission, 2) functional groups introduction, 3) oxidation layer growth, and 4) microscale topology modifications. Further investigations on these mechanisms are required in order to determine the major contributor to the interlayer bonding enhancement.

Moreover, as the results in this research show that interlayer bonding enhancement is not proportional to CPT treatment time, looking for optimal process parameters become an essential task to conduct. A process model needs to be developed in order to simulate the process.

Last but not least, the scalability of the CPT is also required to study. As there exist many types of material, it is important to study the effectiveness of CPT on different material such as ABS or other popular plastics.

5.2.2 Plasma-enhanced FFF process

A fully plasma-integrated FFF printing system is envisioned and a low-fidelity prototype is designed using CAD software, as shown in Figure 24. In an embodiment, a cold plasma discharger is attached alongside the extruder on a rotatable tool holder. After a layer of printing is complete, the plasma discharger will be rotate to the working

position and treat the printed layer. Once treatment is finished, the extruder will move back and immediately start the next layer of printing. This sequence will repeat until the printing completes.

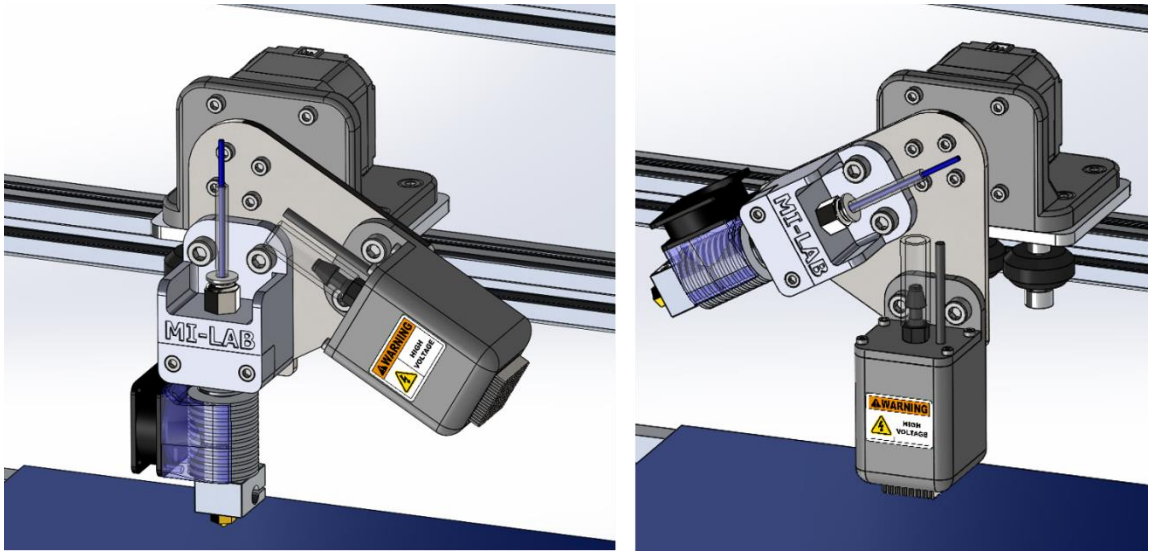

Figure 24 Plasma-enhanced FFF printing system

REFERENCES

[1] J.P. Kruth, M.C. Leu, T. Nakagawa, Progress in Additive Manufacturing and Rapid Prototyping, CIRP Annals 47(2) (1998) 525-540.

[2] T. Campbell, C. Williams, O. Ivanova, B. Garrett, Could 3D printing change the world?, Technologies, potential, and implications of additive manufacturing, (2011).

[3] B. Mueller, Additive Manufacturing Technologies – Rapid Prototyping to Direct Digital Manufacturing, Assembly Automation 32(2) (2012) null.

[4] C.K. Chua, K.F. Leong, 3D Printing and Additive Manufacturing, 2014.

[5] S.S. Crump, Apparatus and method for creating three-dimensional objects, in: USPTO (Ed.) Stratasys Inc USA, 1989.

[6] A. Paesano, Polymeric Additive Manufacturing: Present Status and Future Trends of Materials and Processes, Boeing Technical Journal (2016).

[7] R. Ilardo, C.B. Williams, Design and manufacture of a Formula SAE intake system using fused deposition modeling and fiber-reinforced composite materials, Rapid Prototyping Journal 16(3) (2010) 174-179.

[8] R.K. Chen, Y.-a. Jin, J. Wensman, A. Shih, Additive manufacturing of custom orthoses and prostheses—A review, Additive Manufacturing 12 (2016) 77-89.

[9] A. International, ASTM D638-14 Standard Test Method for Tensile Properties of Plastics, West Conshohocken, PA, 2014.

[10] S.H. Ahn, M. Montero, D. Odell, S. Roundy, P.K. Wright, Anisotropic material properties of fused deposition modeling ABS, Rapid Prototyping Journal 8(4) (2002) 248-257.

[11] K.R. Hart, E.D. Wetzel, Fracture behavior of additively manufactured acrylonitrile butadiene styrene (ABS) materials, Engineering Fracture Mechanics 177 (2017) 1-13.

[12] C.S. Lee, S.G. Kim, H.J. Kim, S.H. Ahn, Measurement of anisotropic compressive strength of rapid prototyping parts, Journal of Materials Processing Technology 187-188 (2007) 627-630.

[13] N. Aliheidari, R. Tripuraneni, A. Ameli, S. Nadimpalli, Fracture resistance measurement of fused deposition modeling 3D printed polymers, Polymer Testing 60 (2017) 94-101.

[14] J.R.C. Dizon, A.H. Espera, Q. Chen, R.C. Advincula, Mechanical characterization of 3D-printed polymers, Additive Manufacturing 20 (2018) 44-67.

[15] M. Domingo-Espin, J.M. Puigoriol-Forcada, A.-A. Garcia-Granada, J. Llumà, S. Borros, G. Reyes, Mechanical property characterization and simulation of fused deposition modeling Polycarbonate parts, Materials & Design 83 (2015) 670-677.

[16] C. Koch, L. Van Hulle, N. Rudolph, Investigation of mechanical anisotropy of the fused filament fabrication process via customized tool path generation, Additive Manufacturing 16 (2017) 138-145.

[17] J.C. Riddick, M.A. Haile, R.V. Wahlde, D.P. Cole, O. Bamiduro, T.E. Johnson, Fractographic analysis of tensile failure of acrylonitrile-butadiene-styrene fabricated by fused deposition modeling, Additive Manufacturing 11 (2016) 49-59.

[18] A.R. Torrado, C.M. Shemelya, J.D. English, Y. Lin, R.B. Wicker, D.A. Roberson, Characterizing the effect of additives to ABS on the mechanical property anisotropy of specimens fabricated by material extrusion 3D printing, Additive Manufacturing 6 (2015) 16-29.

[19] K.M. Rahman, T. Letcher, R. Reese, Mechanical Properties of Additively Manufactured PEEK Components Using Fused Filament Fabrication, (57359) (2015) V02AT02A009.

[20] A. Sung-Hoon, M. Michael, O. Dan, R. Shad, W.P. K., Anisotropic material properties of fused deposition modeling ABS, Rapid Prototyping Journal 8(4) (2002) 248-257.

[21] C. Ziemian, M. Sharma, S. Ziemian, Anisotropic mechanical properties of ABS parts fabricated by fused deposition modelling, Mechanical engineering, InTech2012.

[22] C. Bellehumeur, L. Li, Q. Sun, P. Gu, Modeling of Bond Formation Between Polymer Filaments in the Fused Deposition Modeling Process, Journal of Manufacturing Processes 6(2) (2004) 170-178.

[23] C. McIlroy, P.D. Olmsted, Disentanglement effects on welding behaviour of polymer melts during the fused-filament-fabrication method for additive manufacturing, Polymer 123 (2017) 376-391.

[24] P.K. Gurrala, S.P. Regalla, Part strength evolution with bonding between filaments in fused deposition modelling, Virtual and Physical Prototyping 9(3) (2014) 141-149.

[25] Q. Sun, G.M. Rizvi, C.T. Bellehumeur, P. Gu, Effect of processing conditions on the bonding quality of FDM polymer filaments, Rapid Prototyping Journal 14(2) (2008) 72-80.

[26] C. Casavola, A. Cazzato, V. Moramarco, C. Pappalettere, Orthotropic mechanical properties of fused deposition modelling parts described by classical laminate theory, Materials & Design 90 (2016) 453-458.

[27] T.J. Coogan, D.O. Kazmer, Bond and part strength in fused deposition modeling, Rapid Prototyping Journal 23(2) (2017) 414-422.

[28] A.C. Abbott, G.P. Tandon, R.L. Bradford, H. Koerner, J.W. Baur, Process-structure-property effects on ABS bond strength in fused filament fabrication, Additive Manufacturing 19 (2018) 29-38.

[29] J.F. Rodriguez, J.P. Thomas, J.E. Renaud, Characterization of the mesostructure of fused-deposition acrylonitrile-butadiene-styrene materials, Rapid Prototyping Journal 6(3) (2000) 175-186.

[30] S. Wu, Polymer Interface and adhesion, Marcel Dekker, New York, 1982.

[31] A.K. Sood, R.K. Ohdar, S.S. Mahapatra, Parametric appraisal of mechanical property of fused deposition modelling processed parts, Materials & Design 31(1) (2010) 287-295.

[32] A. Lanzotti, M. Grasso, G. Staiano, M. Martorelli, The impact of process parameters on mechanical properties of parts fabricated in PLA with an open-source 3-D printer, Rapid Prototyping Journal 21(5) (2015) 604-617.

[33] K. Chockalingam, N. Jawahar, J. Praveen, Enhancement of Anisotropic Strength of Fused Deposited ABS Parts by Genetic Algorithm, Materials and Manufacturing Processes 31(15) (2016) 2001-2010.

[34] J. Torres, M. Cole, A. Owji, Z. DeMastry, A.P. Gordon, An approach for mechanical property optimization of fused deposition modeling with polylactic acid via design of experiments, Rapid Prototyping Journal 22(2) (2016) 387-404.

[35] M. Spoerk, F. Arbeiter, H. Cajner, J. Sapkota, C. Holzer, Parametric optimization of intra- and inter-layer strengths in parts produced by extrusion-based additive manufacturing of poly(lactic acid), Journal of Applied Polymer Science 134(41) (2017) 45401.

[36] S. Shaffer, K. Yang, J. Vargas, M.A. Di Prima, W. Voit, On reducing anisotropy in 3D printed polymers via ionizing radiation, Polymer 55(23) (2014) 5969-5979.

[37] J. Du, Z. Wei, X. Wang, J. Wang, Z. Chen, An improved fused deposition modeling process for forming large-size thin-walled parts, Journal of Materials Processing Technology 234 (2016) 332-341.

[38] A.K. Ravi, A. Deshpande, K.H. Hsu, An in-process laser localized pre-deposition heating approach to inter-layer bond strengthening in extrusion based polymer additive manufacturing, Journal of Manufacturing Processes 24 (2016) 179-185.

[39] V. Kishore, C. Ajinjeru, A. Nycz, B. Post, J. Lindahl, V. Kunc, C. Duty, Infrared preheating to improve interlayer strength of big area additive manufacturing (BAAM) components, Additive Manufacturing 14 (2017) 7-12.

[40] J. Wang, H. Xie, Z. Weng, T. Senthil, L. Wu, A novel approach to improve mechanical properties of parts fabricated by fused deposition modeling, Materials & Design 105 (2016) 152-159.

[41] C.B. Sweeney, B.A. Lackey, M.J. Pospisil, T.C. Achee, V.K. Hicks, A.G. Moran, B.R. Teipel, M.A. Saed, M.J. Green, Welding of 3D-printed carbon nanotube–polymer composites by locally induced microwave heating, Science Advances 3(6) (2017).

[42] W. Jo, O.-C. Kwon, M.-W. Moon, Investigation of influence of heat treatment on mechanical strength of FDM printed 3D objects, Rapid Prototyping Journal 24(3) (2018) 637-644.

[43] F. Lederle, F. Meyer, G.-P. Brunotte, C. Kaldun, E.G. Hübner, Improved mechanical properties of 3D-printed parts by fused deposition modeling processed under the exclusion of oxygen, Progress in Additive Manufacturing 1(1) (2016) 3-7.

[44] H. Narahara, Y. Shirahama, H. Koresawa, Improvement and Evaluation of the Interlaminar Bonding Strength of FDM Parts by Atmospheric-Pressure Plasma, Procedia CIRP 42 (2016) 754-759.

[45] H. Abourayana, P. Dobbyn, D. Dowling, Enhancing the mechanical performance of additive manufactured polymer components using atmospheric plasma pre-treatments, Plasma Processes and Polymers 15(3) (2018) 1700141.

[46] A. Garg, A. Bhattacharya, A. Batish, Chemical vapor treatment of ABS parts built by FDM: Analysis of surface finish and mechanical strength, The International Journal of Advanced Manufacturing Technology 89(5) (2017) 2175-2191.

[47] N.A. Nguyen, C.C. Bowland, A.K. Naskar, A general method to improve 3D-printability and inter-layer adhesion in lignin-based composites, Applied Materials Today 12 (2018) 138-152.

[48] G. Li, J. Zhao, W. Wu, J. Jiang, B. Wang, H. Jiang, J. Fuh, Effect of Ultrasonic Vibration on Mechanical Properties of 3D Printing Non-Crystalline and Semi-Crystalline Polymers, Materials 11(5) (2018) 826.

[49] C. Duty, J. Failla, S. Kim, T. Smith, J. Lindahl, A. Roschli, B. Post, L. Love, V. Kunc, Z-Pinning Approach for Reducing Mechanical Anisotropy of 3D Printed Parts, Proc. The Solid Freeform Fabrication Symposium, 2018 (2018).

[50] N.P. Levenhagen, M.D. Dadmun, Interlayer diffusion of surface segregating additives to improve the isotropy of fused deposition modeling products, Polymer 152 (2018) 35-41.

[51] N.P. Levenhagen, M.D. Dadmun, Bimodal molecular weight samples improve the isotropy of 3D printed polymeric samples, Polymer 122 (2017) 232-241.

[52] A. Armillotta, M. Bellotti, M. Cavallaro, Warpage of FDM parts: Experimental tests and analytic model, Robotics and Computer-Integrated Manufacturing 50 (2018) 140-152.

[53] E. Bormashenko, G. Whyman, V. Multanen, E. Shulzinger, G. Chaniel, Physical mechanisms of interaction of cold plasma with polymer surfaces, Journal of Colloid and Interface Science 448 (2015) 175-179.

[54] A. Jordá-Vilaplana, V. Fombuena, D. García-García, M.D. Samper, L. Sánchez-Nácher, Surface modification of polylactic acid (PLA) by air atmospheric plasma treatment, European Polymer Journal 58 (2014) 23-33.

[55] L. Bárdos, H. Baránková, Cold atmospheric plasma: Sources, processes, and applications, Thin Solid Films 518(23) (2010) 6705-6713.

[56] J. Chang, P.A. Lawless, T. Yamamoto, Corona discharge processes, IEEE Transactions on Plasma Science 19(6) (1991) 1152-1166.

[57] S.A. Dion, A.S. David, F. Alexander, F. Bakhtier, Atmospheric pressure dc corona discharges: operating regimes and potential applications, Plasma Sources Science and Technology 18(3) (2009) 035016.

[58] I.G. Valentin, J.P. Gerhard, The development of dielectric barrier discharges in gas gaps and on surfaces, Journal of Physics D: Applied Physics 33(20) (2000) 2618.

[59] U. Kogelschatz, Dielectric-Barrier Discharges: Their History, Discharge Physics, and Industrial Applications, Plasma Chemistry and Plasma Processing 23(1) (2003) 1-46.

[60] B. Ronny, Dielectric barrier discharges: progress on plasma sources and on the understanding of regimes and single filaments, Plasma Sources Science and Technology 26(5) (2017) 053001.

[61] J. Winter, R. Brandenburg, K.D. Weltmann, Atmospheric pressure plasma jets: an overview of devices and new directions, Plasma Sources Science and Technology 24(6) (2015) 064001.

[62] S.K. Pankaj, C. Bueno-Ferrer, N.N. Misra, V. Milosavljević, C.P. O'Donnell, P. Bourke, K.M. Keener, P.J. Cullen, Applications of cold plasma technology in food packaging, Trends in Food Science & Technology 35(1) (2014) 5-17.

[63] T. Dufour, J. Minnebo, S.A. Rich, E.C. Neyts, A. Bogaerts, F. Reniers, Understanding polyethylene surface functionalization by an atmospheric He/O 2 plasma through combined experiments and simulations, Journal of Physics D: Applied Physics 47(22) (2014) 224007.

[64] K. Terpiłowski, D. Rymuszka, Surface free energy changes of polyethylene after plasma treatment, in: A. Mendez-Vilas, A. Solano-Martin (Eds.), Polymer science: research advances, practical applications and educational aspects, Formatex Research Center, Spain, 2016, pp. 498-505.

[65] A. International, ASTM 3163 Standard Test Method for Determining Strength of Adhesively Bonded Rigid Plastic Lap-Shear Joints in Shear by Tension Loading, West Conshohocken, PA, 2014.

[66] A. International, ASTM 1876 Standard Test Method for Peel Resistance of Adhesives (T-Peel Test), West Conshohocken, PA, 2015.

[67] A. International, ASTM 4541-17 Standard Test Method for Pull-Off Strength of Coatings Using Portable Adhesion Testers, West Conshohocken, PA.

[68] K. Cantekin, S. Avci, Evaluation of shear bond strength of two resin-based composites and glass ionomer cement to pure tricalcium silicate-based cement (Biodentine®), Journal of Applied Oral Science 22 (2014) 302-306.

[69] C. Laux, Radiation and nonequilibrium collisional-radiative models, 2000.

[70] S. David, F. Bakhtier, F.G. Alexander, A.F. Alexander, Spectroscopic studies and rotational and vibrational temperature measurements of atmospheric pressure normal glow plasma discharges in air, Plasma Sources Science and Technology 15(4) (2006) 818.

[71] A. International, ASTM D7334-08 Standard Practice for Surface Wettability of Coatings, Substrates and Pigments by Advancing Contact Angle Measurement, West Conshohocken, PA, 2013.

[72] C.B. Bucknall, R.R. Smith, Stress-whitening in high-impact polystyrenes, Polymer 6(8) (1965) 437-446.